SA-TIED
Southern Africa – Towards Inclusive Economic Development

The changing nature of hydroclimatic risks across Southern Africa

C. Adam Schlosser, Andrei Sokolov, Ken Strzepek, Tim Thomas, Xiang Gao, and Channing Arndt

SA-TIED Working Paper #101 | March 2020

UNITED NATIONS UNIVERSITY UNU-WIDER
national treasury Department: National Treasury REPUBLIC OF SOUTH AFRICA
INTERNATIONAL FOOD POLICY RESEARCH INSTITUTE IFPRI
& evaluation Department: Planning, Monitoring and Evaluatio REPUBLIC OF SOUTH AFRICA
the dti Department: Trade and Industry REPUBLIC OF SOUTH AFRICA
SARS
TIPS

About the programme

Southern Africa –Towards Inclusive Economic Development (SA-TIED)

SA-TIED is a unique collaboration between local and international research institutes and the government of South Africa. Its primary goal is to improve the interface between research and policy by producing cutting-edge research for inclusive growth and economic transformation in the southern African region. It is hoped that the SA-TIED programme will lead to greater institutional and individual capacities, improve database management and data analysis, and provide research outputs that assist in the formulation of evidence-based economic policy.

The collaboration is between the United Nations University World Institute for Development Economics Research (UNU-WIDER), the National Treasury of South Africa, the International Food Policy Research Institute (IFPRI), the Department of Monitoring, Planning, and Evaluation, the Department of Trade and Industry, South African Revenue Services, Trade and Industrial Policy Strategies, and other universities and institutes. It is funded by the National Treasury of South Africa, the Department of Trade and Industry of South Africa, the Delegation of the European Union to South Africa, IFPRI, and UNU-WIDER through the Institute's contributions from Finland, Sweden, and the United Kingdom to its research programme.

Copyright © The Author(s) 2020

Corresponding author: ifpri@cgiar.org

The views expressed in SA-TIED working papers are those of the author(s) and do not necessarily represent the views of the programme partners or its donors.

IFPRI

Towards Inclusive Economic Development in Southern Africa

SA-TIED | Working Paper #101 | March 2020

The changing nature of hydroclimatic risks across Southern Africa

C. Adam Schlosser, Andrei Sokolov, Ken Strzepek, Tim Thomas, Xiang Gao, and Channing Arndt

ABSTRACT

This study presents results from a large ensemble of projected changes in seasonal precipitation and near-surface air temperature changes for the nation of South Africa. The ensemble is based on a combination of pattern-change responses derived from the Coupled Model Intercomparison Project Phase 5 (CMIP-5) climate models along with the Massachusetts Institute of Technology Integrated Global Systems Model (MIT-IGSM), an intermediate complexity earth-system model coupled to a global economic model that evaluates uncertainty in socio-economic growth, anthropogenic emissions, and global environmental response. Numerical experimentation with the MIT-IGSM considered four scenarios of future climate and socio-economic development to span a range of possible global actions to abate greenhouse gas emissions through the 21st century. We evaluate distributions of surface-air temperature and precipitation change over three regions across South Africa: western (WSoAfr), central (CSoAfr), and eastern (ESoAfr) South Africa. In all regions, by mid-century, we find a strong likelihood (greater than 50%) that temperatures will rise considerably higher than the current climate's range of variability (a threefold increase over the current climate's two-standard deviation range of variability). In addition, scenarios that consider more aggressive global climate targets (e.g. 2C and 15C scenarios) all but eliminate the risk of these acutely salient temperature increases. For precipitation, there is a preponderance of risk toward decreased precipitation (3 to 4 times higher than increased) for western and central parts of South Africa. There is a clear benefit seen within the evolving hydroclimatic risks as a result of strong climate targets, such as limiting the global climate warming to 1.5˚C by 2100. We find that the risk of precipitation changes in the 15C scenario toward the end of this century (2065-2074) is nearly identical to that seen in the REF scenario during the 2030s. Thus, the climate risk that may be experienced in a decade as a result of current global actions to reduce emissions could be delayed by 30 years, and would provide invaluable lead-time for national efforts to be put in place to prepare, fortify, and/or adapt to these changing environments of risk.

1 INTRODUCTION

Evidence is mounting that Africa's climate is changing and that these trends will continue through the 21st century (e.g. Niang et al., 2014). However, a range of outcomes in climate-change projections derived from individual assessments exist and studies performed with a small sample size of model simulations remain somewhat inconclusive (e.g. Cretat et al., 2012). While current efforts to provide more spatially refined climate-change information over Africa are ongoing (e.g. Lennard et al., 2018), these efforts require computationally expensive and time consumptive models to be exercised. Therefore, there remains a distinct need for efficient methods that provide comprehensive samples of all the plausible model solutions to future climate. Further, these methods should also have the ability to consider a number of different scenarios that consider a range of global emissions pathways and/or climate targets and provide spatial details of climate that are commensurate to the needs of regional impact studies. This study analyses the likelihood of changes in precipitation and surface-air temperature in the coming decades and into the latter half of this century for the greater southern Africa region with a regional emphasis over South Africa. We present a technique used to construct pattern-kernels of climate change based on information of regional change from climate models (Schlosser et al., 2012) and the application of these patterns of change to downscale the zonal output of the MIT Integrated Global System Model (Reilly et al., 2018). Given the large-ensemble approach employed by the IGSM, the fusion of these pattern-kernels to the IGSM simulations results in frequency (or likelihood) distributions. We evaluate these distributions for temperature and precipitation averaged over three selected regions over South Africa that are chosen to correspond with important climatic classification. We evaluate and identify the salient shifts in these derived distributions from a reference emission scenario to moderate to aggressive climate-stabilization policies. We close with summary remarks and discussion of ongoing work and applications.

2 ASSESSMENT OF REGIONAL CLIMATE SHIFTS

2.1 Region of study

The overall area of study (Figure 1) is an extension and complement to prior work (Arndt et al., 2019; Schlosser and Strzepek, 2015; Fant et al., 2015) that provides multi-sector socio-economic-environmental assessments of climate risks for developing nations across Africa, and the effectiveness of low-carbon pathways to reduce risks. This study will present a broad view of potential climate shifts over southern Africa and focus on two hydro-climatic variables precipitation (P) and near-surface air temperature (T_a), and these will be used as inputs for assessments of climate-change impacts to agriculture yields (Thomas et al. 2020, forthcoming) within South Africa. In this vein, we focus on three sub-regions across South Africa (denoted in Figure 1) and provide a more quantitative analysis of climate risk and the impact of low-carbon pathways across three decadal epochs (2030s, 2050s, and 2065-75). A description of the model experimentation and methodology is provided in the next section. Below we describe some of the distinct seasonal features of temperature and precipitation of the current climate that are aligned and distinguish our three regional areas of focus: eastern, central, and western South Africa (ESoAfr, CSoAfr, and WSoAfr, respectively). Our historical assessment is based on the observations taken from the Global Precipitation Climatology Project (GPCP, Huffman et al, 2009, and updates by Adler et al., 2018) as well as surface-air temperature from the Climate Research Unit (CRU, e.g. Osborn et al., 2014).

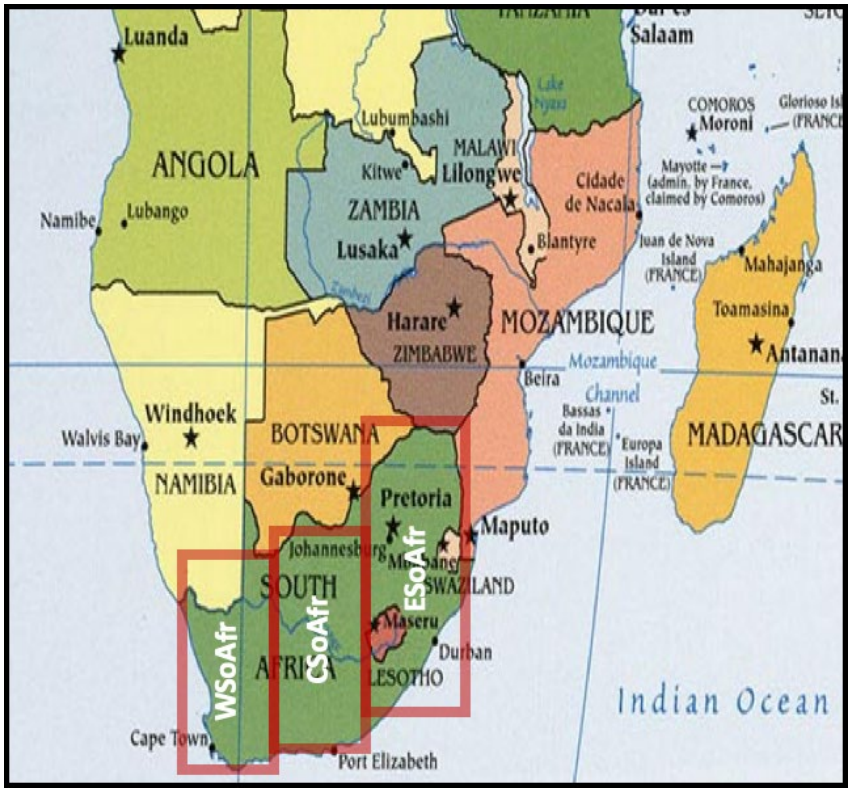

Figure 1. Map of the overall area of study – areas of regional focus within South Africa are indicated by red boxes. These regions cover the western (WSoAfr), central (CSoAfr), and eastern (ESoAfr) sections of South Africa. This map has been adapted from an image archive available at https://www.worldatlas.com/webimage/countrys/afpoliticallg.htm.

The western South Africa (WSoAfr) region is primarily distinguished by the persistently lowest rates of precipitation across all seasons (Figure 2 and Table 1). This also results in the weakest amplitude in the seasonal cycle of precipitation. Further, due to the localized precipitation maxima over the Cape Town area during JJA, the seasonal cycle of precipitation averaged over the WSoAfr region is opposite in phase to the CSoAfr and ESoAfr regions. In contrast, the ESoAfr region experiences the highest precipitation rates during the summer (DJF) season, and the transition to the wet season is abrupt as the landscape of spring season (SON) precipitation is very similar to the winter (JJA). Given these strong contrasts between the western and eastern flanks of South Africa, the CSoAfr region represents a distinct transition region, with a seasonal cycle that is in phase with but an amplitude that is almost half that of ESoAfr. The seasonality of surface-air temperature exhibits more consistency across these regions compared to precipitation (Figure 3 and Table 1). The area-averaged, seasonal cycles are all in phase and comparable in terms of magnitude. A notable distinction is that ESoAfr experiences the warmest temperatures during the winter season (JJA), yet it contains the largest area of coolest temperatures (along its inland western flank) as well as the location of the coolest temperature for the region. However, this is more than offset by the warmest temperatures along its coastal boundary. In contrast, the WSoAfr and CSoAfr regions do not experience as strong a contrast in surface-air temperatures.In order to gauge a degree of salience to the changes produced by the ensemble scenarios of change (described in the next sections), we have also assessed the interdecadal standard deviation of the seasonal, area-averaged quantities (Table 1, in italics). For surface-air temperature, the standard deviations are very consistent across seasons and the regions. For precipitation, the highest variabilities follow the region and season of highest mean (CSoAfr and ESoAfr during DJF). In our assessment of the distribution of changes across the 21st century (Section 2.4), we will highlight the portions of the distributions that are in exceedance to these variance statistics, and in this way, represent the risk of salient change.

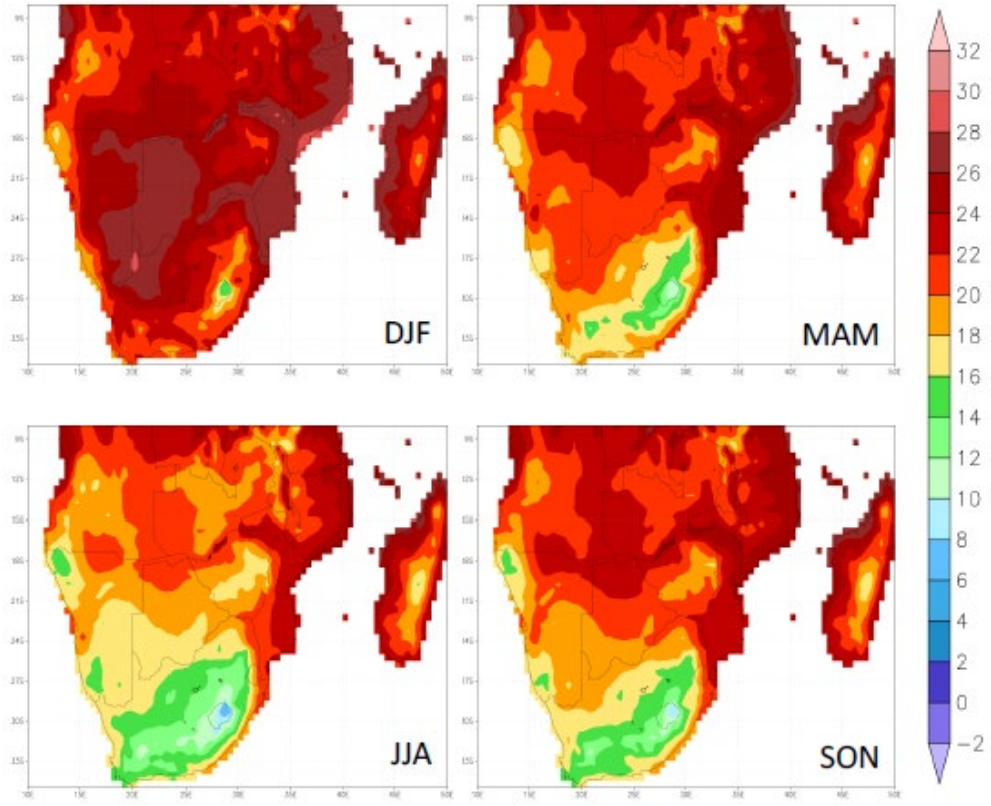

Figure 2: Seasonal averaged (1979-2009) maps of surface-air temperature for southern Africa. Results are shown for: a) December-February; b) March-May; c) June-August; and d) September-November. Units are in °C. Temperature data is based on the Climate Research Unit (CRU, Jones et al., 1999) data archive.

Table 1: Mean (bold) and standard deviations (italics) of area-averaged precipitation and surface-air temperature for the western, central, and eastern South Africa regions (WSoAfr, CSoAfr, and ESoAfr respectively) of study. Results are presented for two seasonal mean periods: December-February (DJF) and June-August (JJA). The diagnostics of precipitation (units in mm/decads, decad=10 days) are based on the Global Precipitation Climatology Project (units in ˚C), and surface-air temperature is based on observations assembled by the Climate Research Unit (CRU). See text for citations to data. Statistics span the years 1979-2019, and note that the standard deviation estimates are based across decadal means for each season so as to serve as a baseline for the decadal mean changes assessed in the 21st century scenario projections.

		WSoAfr	*CSoAfr*	*ESoAfr*
Precipitation	DJF	**7.3** ± *0.7*	**23.3** ± *1.5*	**39.5** ± *1.7*
	JJA	**10.0** ± *0.5*	**4.6** ± *1.0*	**5.2** ± *0.7*
Temperature	DJF	**23.5** ± *0.3*	**23.0** ± *0.3*	**22.7** ± *0.2*
	JJA	**11.9** ± *0.3*	**11.1** ± *0.3*	**13.9** ± *0.3*

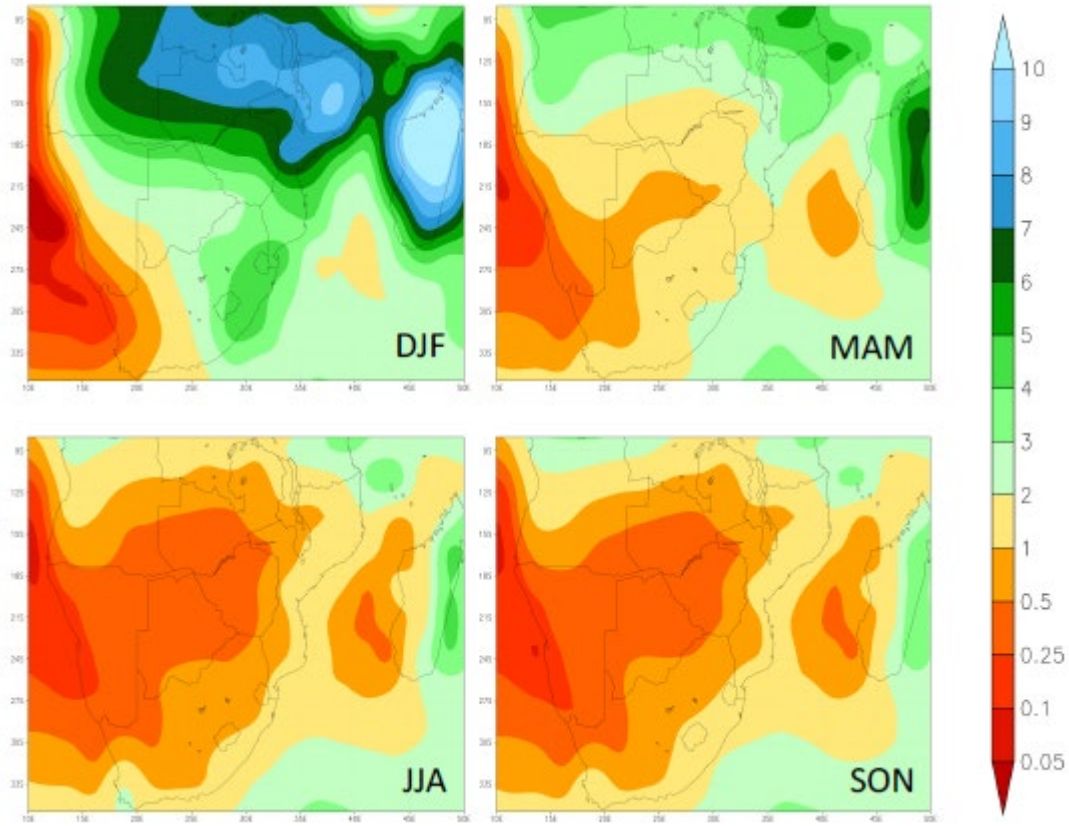

Figure 3: Seasonal averaged maps (1979-2009) of precipitation (mm/day) for northern Africa. Results are shown for: December-February (DJF, upper left panel); b) March-May (MAM, upper right panel); c) June-August (JJA, lower left panel); and d) September-November (SON, lower right panel). Units are in mm/day. Results are based on the data from the Global Precipitation Climatology Project (GPCP, Huffman et al., 2007).

2.2 Scenarios of global change

The set of scenarios for this exercise was selected from the 2018 Food, Energy, Water, and Climate Outlook produced by the MIT Joint Program on the Science and Policy of Global Change (Reilly et al., 2018). The scenarios, each run under a large ensemble of 400 members, consider a broad range of uncertainties Earth systems' behavior and response to natural and anthropogenic drivers (e.g. Sokolov et al., 2018 and Libardoni et al., 2018), and also span a range of global emissions policies and are based on a regionally detailed, multi-sector, economy-wide model that includes pricing of fossil fuels, fossil resources, and vintage capital in capital intensive sectors (e.g. Chen et al., 2016). Under policy scenarios, prematurely retired capital stock and the need to replace conventional energy sources with more expensive, low-carbon options draw investment resources away from other sectors of the economy and, thus, have an impact on GDP growth in mitigation scenarios. The reduced GDP thereby reduces investment overall in the mitigation scenarios. However, it is reallocated toward those energy sources that meet the emissions reduction targets at least cost.

Four scenarios, developed to span a range of possible global actions to abate greenhouse gas emissions over the coming century, were used to explore climate-change risks.

Reference (REF)

This scenario has no explicit climate mitigation policies anywhere in the world. Thus, it represents a world in which there is no Paris Agreement and no alternative action towards reducing emissions for the sake of limiting climate change. However, it includes some energy policies such as fuel economy standards, renewable electricity requirements, and the gradual phase-out of old coal power plants that are presently occurring with various motivations. These motivations include reducing imported oil

dependence, using less of exhaustible resources, or to reducing conventional pollutants. Such efforts may in part reflect concerns about climate change, but the policies have no specific greenhouse gas emissions targets. The REF serves as a baseline scenario because of its simplicity. Metrics from the other scenarios are often presented as the difference between another scenario and the REF scenario. It provides the upper assessment of our modeled physical risks.

Paris forever (PF)

Countries meet the mitigation targets in their Nationally Determined Contributions (NDCs) and continue to abide by them through the end of the century. The Paris Agreement includes NDCs submitted at the 2015 Paris Conference of the Parties (COP) of the Framework Convention on Climate Change (FCCC). These NDCs—aimed at the reduction of CO_2 and other GHG emissions—generally deepened and extended through 2030 those made at the 2009 Copenhagen COP through 2020. These reductions are typically expressed as (1) an absolute emissions target (ABS), measured as an annual level of emissions measured in Mt, (2) a percentage reduction from a pre-determined baseline, which can easily be converted into an absolute emissions target, or (3) an emissions intensity target (INT), measured as emissions in relation to GDP.

2C

This scenario aims to limit climate warming to no higher than a 2˚C global average at 2100. This is achieved by implementing a globally coordinated, smoothly rising carbon price – such that emissions are reduced. Variations in mitigation policies result in the overall uncertainty of different patterns of resource and energy use, different choices of technology, and drag on overall economic growth. This is also combined with the uncertainty of the global climate response that is represented in the MIT Earth System Model (MESM, Sokolov et al., 2019). As described in Reilly et al. (2018) – these co-evolving uncertainties projected within a Latin-hypercube sampling results in an overall probability of achieving the target at 66%.

15C

Similar to the 2C, this scenario aims to limit climate warming to no higher than 1.5˚C global average at 2100. Under the similar Latin-hypercube sampling of structural uncertainties within the Earth and human model systems, this results in a 50% probability of achieving the climate target (i.e. 200 of the 400-member ensemble meets the target).

These scenarios result in distinct distributions of global averaged changes in key climate variables (Figure 4, shown are results for decadal mean changes in the 2050s). The mid-century impact of the more aggressive climate-based targets (i.e. 15C and 2C scenarios) is distinguished by the majority of their distribution of outcomes falling outside the distribution of the REF scenario. In addition, shifts in the modal value of change, the percentage of the distribution at the modal value, as well as the total range of outcomes (i.e. width of the distribution) highlight the notable impact of the aggressive climate targets at reducing (and eliminating) the risk of strongest changes. The PF scenario, which captures the current global commitments to reduce emissions (under the Paris Agreement), shows a discernible shift toward lower risks of change, yet considerable overlap (particularly for surface-air temperature) with the REF distributions remain by mid-century. Given all these considerations, we can then gauge the extent of how these global results translate into regional features of risk through a procedure described in the next section.

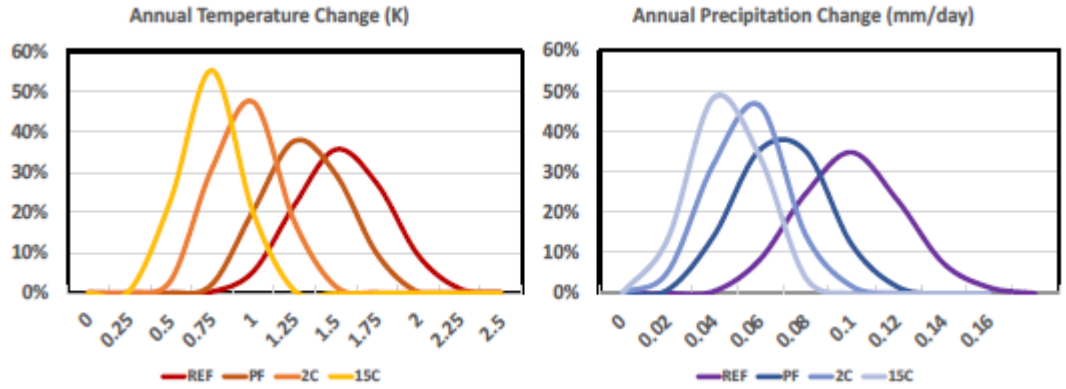

Figure 4. Global averaged results (Antarctica and Arctic Ocean excluded) from the MIT Earth-System Model (MESM) show the distribution of mid-century decadalaveraged changes (2050-2059) in surface-air temperature (left panel) and precipitation (right panel) relative to the end of the 20th-century. Shown are the results from the four scenarios of change performed by the MIT Integrated Global System Model (IGSM) framework: Reference (REF), Paris Forever (PF), and the 2°C and 1.5°C climate targets (2C and 15C, respectively). Refer to text for a description of the scenarios. Note for visual clarity (to highlight the impact of the scenarios), these distributions are shown as curve fits to the binned distributions of outcome values (denoted by the abscissa values).

2.3 Regional climate-change pattern kernels

Our construction of the regional distributions of change follows previous work presented by Schlosser *et al.* (2012). The underlying motivation for this approach is driven by the MIT Earth Systems Model (MESM, Sokolov *et al.*, 2018) providing probabilistic projections of T_a and precipitation at the zonal level of detail. In to provide regional texture to these outcomes, we must expand this information across longitudes. The technique employs a Taylor expansion technique. This transformation results in the construction of climate-change pattern kernels - and these kernels are scaled by global temperature change, and the numerical relationship can be expressed as:

$$V_{x,y}^{IGSM}(\Delta T_{Global}) = C_{x,y}\Big|_{t_0} \overline{V}_y^{IGSM} + \left[\frac{dC_{x,y}}{dT_{Global}} \Delta T_{Global}^{IGSM}\right] \overline{V}_y^{IGSM} \quad (1)$$

where $C_{x,y}\Big|_{t_0}$ is the climatological downscaling transformation coefficient (altering the zonal mean value to assign a particular value for a longitudinal point along the zonal band) for any reference time period, and we base this climatological coefficient on observational data. The observational data sources are the same as those used in the prior section that summarized the historical climates for our study region (GPCP and CRU). The projected change in globally averaged temperature, ΔT_{Global}, is relative to a reference or climatological period (1980-1999). The derivative of these transformation coefficients, $\frac{dC_{x,y}}{dT_{Global}}$, for any point (x,y) are discretely estimated from climate model information (for further details, see Schlosser *et al*., 2012). Therefore, the $\frac{dC_{x,y}}{dT_{Global}}$ terms serve as "pattern-change kernels" (PCKs) of regional climate shifts. We construct a set of these PCKs based on the results from the Coupled Model Intercomparison Project Phase 5 (CMIP5, Taylor et al., 2012), and as a result, this provides the regional basis for the large ensembles that allow us to construct distributions of change. The CMIP5 model archive provides a comprehensive set of outputs from climate and Earth-system models that have been developed at institutes across the international scientific community. In some cases, these institutes submitted multiple results that were conducted by their model under a variety of different configurations (e.g. different spatial resolutions and/or various parameterization prescriptions). In constructing this meta-ensemble, we did not incorporate "sibling" model results and

instead selected only one set of model results per institute to determine a representative PCK. This was done in order to avoid biasing in the meta-distribution that would result from using "sibling" PCKs (and thereby inappropriately stacking a regional pattern of change). Given the problematic nature of assessing the relative fidelity climate model projections (e.g. Reifen and Toumi, 2009), there was no preferential selection to one model result (e.g. the highest spatial resolution) when multiple configurations were available from an institute. This was also done so as to avoid any other possible sources of biasing when deriving these PCKs across all the models/institutes, and to achieve a diverse sampling of outcomes. As a result, the model results from 17 distinct institutes that participated in the CMIP5 exercise were used. Each of the PCKs were constructed at the native model resolution, and then interpolated to a 2˚x2.5˚ common grid, which was commensurate with the coarsest model grid from the CMIP5 model pool. Combined with the 400 members of a MESM model scenario via (1) to obtain patterns of change results in a meta-ensemble of 6,800 members per scenario. This 6,800 member meta-ensemble we refer to as a "hybrid frequency distribution" (HFD), and it is this set of results that is used as the basis of our risk quantification, and the impact of global policy and climate targets, in the regional analysis. As a precursory assessment, we summarize the model-mean, consensus and diversity of the PFKs across the CMIP5 models as well as the corresponding results from the MESM simulations.

2.3.1 Temperature

Overall, the CMIP5 model-mean of $\frac{dC_{x,y}}{dT_{Global}}$ (or PCK) for T_a (Figure 5) exhibits a distinct "colder ocean and warmer land" (COWL) pattern (e.g. Broccoli *et al*., 1998) across all seasons. This overall pattern is seen for all seasons, but the extent and geographic center of the maxima varies. Although not shown, the MESM scenarios' ensembles produce zonal profiles of warming that are fairly constant across the latitude bands that span this region. As described in the prior section, the effect of this PCK is to then produce an enhanced warming over land as global (and zonal) temperatures rise. This relative warming is at its greatest spatial extent in the spring (SON), and at its weakest during summer (DJF) with commensurate conditions into the fall season (MAM). While the model-mean PCKs suggest that this enhanced warming is consistent across all land areas, a closer inspection of the individual model PCKs (Figure 6) indicates there are locations where a local buffering effect would be imposed upon the global (and zonal) warming profiles produced. In two particular model cases (for DJF), this opposing relative trend spans almost the entirety of the ESoAfr region for one model and the WSoAfr region for the other. With respect to our regional focus over South Africa, other models show isolated buffering patterns to warming that are confined to a shallow inland extent from a coastline.

2.3.2 Precipitation

The model-mean as well as inter-model features of the PCKs for precipitation (Figure 7) show a greater degree of heterogeneity (as compared to temperature) across all seasons and regions. However, the most persistent feature is the PCKs imposing a relatively weaker precipitation rate as climate warms across all of the WSoAfr region for all seasons. In contrast, the WSoAfr region exhibits varying degrees of a dipole-like pattern across seasons (except MAM), in which the model-mean PCK would impart a relative enhancement across its southern half and a relative weakening in the northern half of precipitation rates. The CSoAfr region shares features with either ESoAfr or WSoAfr depending on the season. In the cold season (JJA), the model-mean pattern imparts relatively weaker precipitation rates (similar to WSoAfr), and for the remaining seasons its PCK predominantly resembles the landscape of the ESoAfr in sign and/or overall pattern orientation (i.e. north-south oriented gradient). Notwithstanding these common features in the model-mean results, the prominent feature to the precipitation PCKs (particularly in light of the temperature PCKs) lies in the explicit inter-model features (summarized by Figures 8-10).

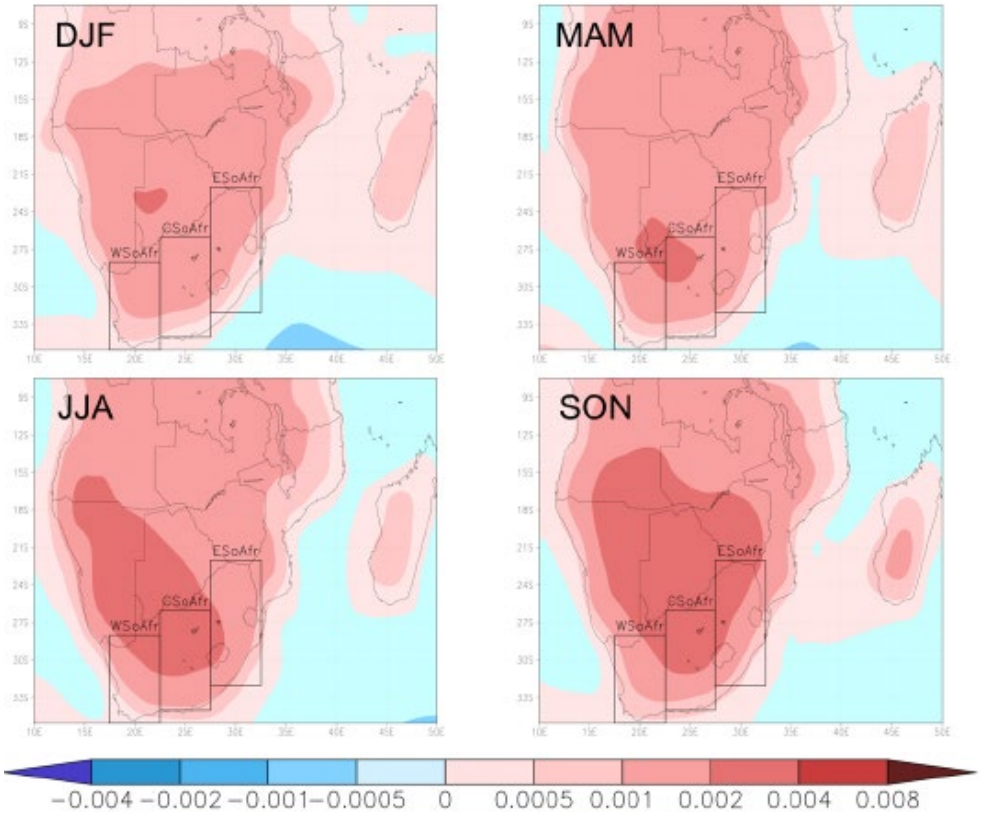

Figure 5: Maps of the pattern-change kernel (PCK) coefficients, $dC_{x,y}/dT_{Global}$ (units of K^{-1}) over southern Africa for surface-air temperature averaged over the results from the CMIP5 climate models. Shown are the seasonally averaged pattern shifts for: December-February (DJF, upper left), March-May (MAM, upper right), June-August (JJA, lower left), and September-November (SON, lower right). In each frame, the three regions of focus over South Africa (WSoAfr, CSoAfr, and ESoAfr) are denoted.

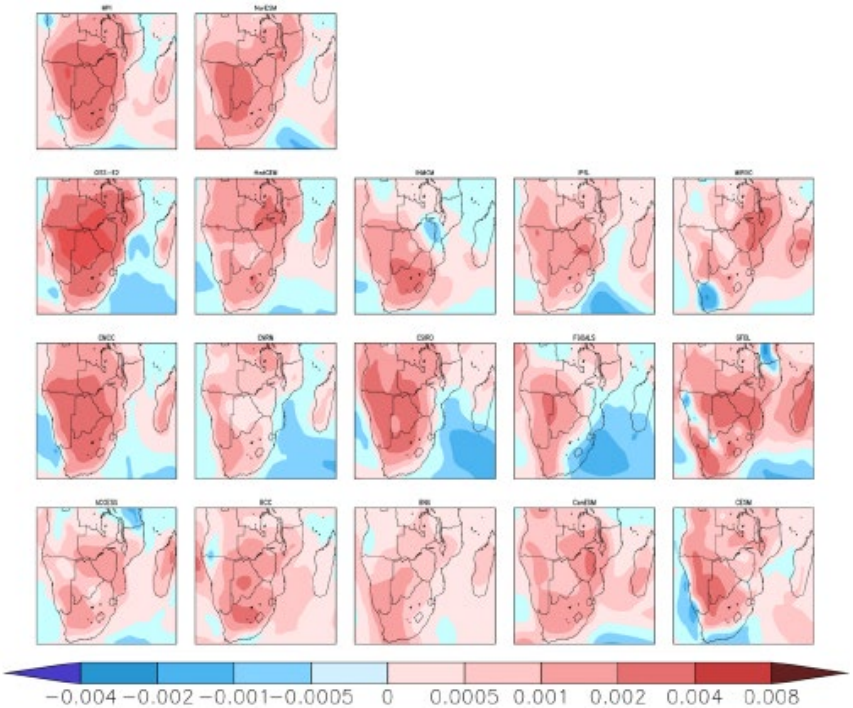

Figure 6: Maps of the pattern-change kernels (PCKs) coefficients, $dC_{x,y}/dT_{Global}$ (units of K^{-1}) over southern Africa for surface-air temperature. Shown are the results for each model of the CMIP5 collection of the seasonally averaged pattern shifts for December-February (DJF).

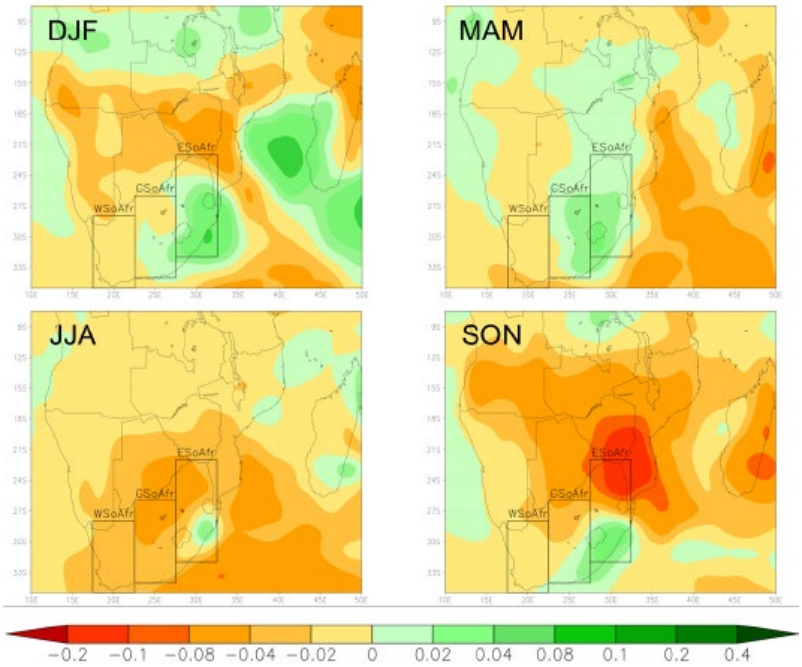

Figure 7: Maps of the pattern-change kernel (PCK) coefficients, $dC_{x,y}/dT_{Global}$ (units of K^{-1}) over southern Africa for surface-air temperature averaged over the results from the CMIP5 climate models. Shown are the seasonally averaged pattern shifts for: December-February (DJF, upper left), March-May (MAM, upper right), June-August (JJA, lower left), and September-November (SON, lower right). In each frame, the three regions of focus over South Africa (WSoAfr, CSoAfr, and ESoAfr) are denoted.

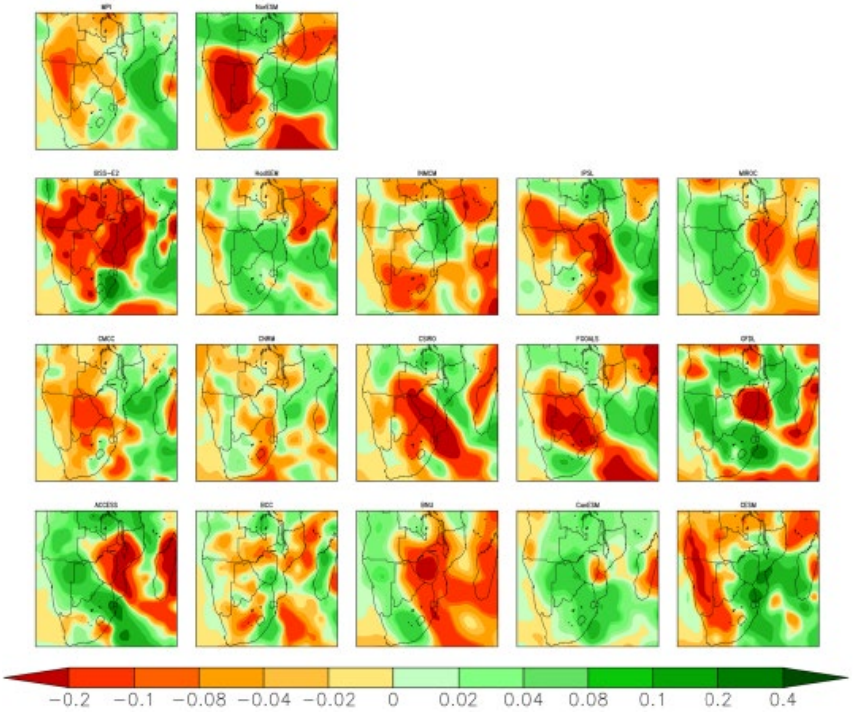

Figure 8: Maps of the pattern-change kernels (PCKs) coefficients, $dC_{x,y}/dT_{Global}$ (units of K^{-1}) over southern Africa for precipitation. Shown are the results for each model of the CMIP5 collection of the seasonally averaged pattern shifts for December-February (DJF).

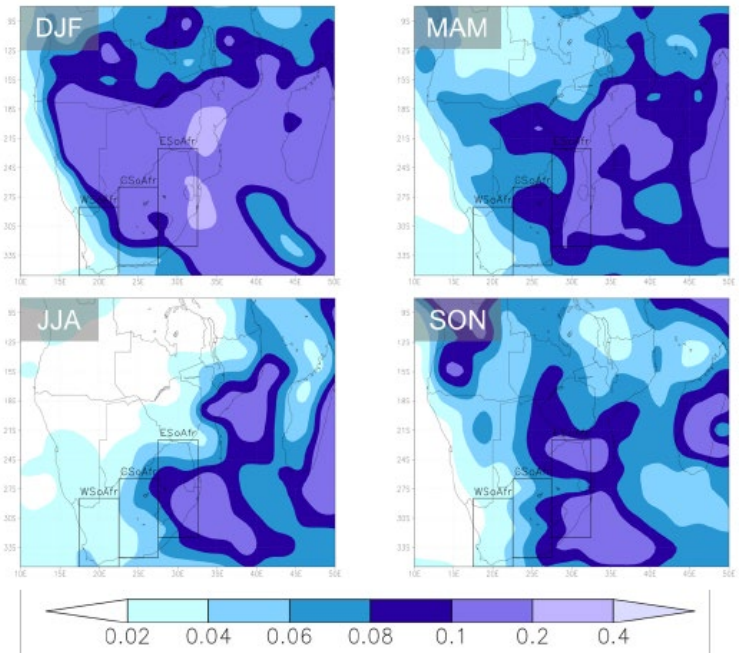

Figure 9: Maps of the inter-model standard deviations of pattern-change kernel (PCK) coefficients, $dC_{x,y}/dT_{Global}$ (units of K^{-1}) over southern Africa for precipitation averaged over the results from the CMIP5 climate models. Shown are the seasonally averaged pattern shifts for: December-February (DJF, upper left), March-May (MAM, upper right), June-August (JJA, lower left), and September-November (SON, lower right). In each frame, the three regions of focus over South Africa (WSoAfr, CSoAfr, and ESoAfr) are denoted.

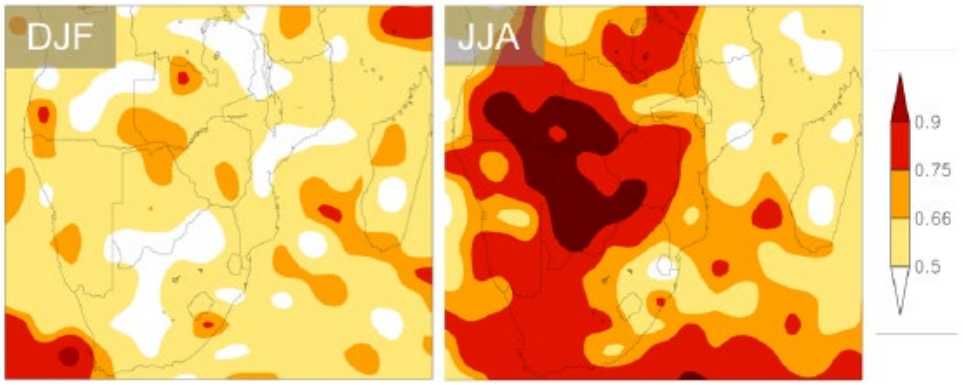

Figure 10. Maps that summarize the sign-agreement in pattern-change kernel (PCK) coefficients, $dC_{x,y}/dT_{Global}$ (units of K^{-1}) over southern Africa for precipitation averaged over the results from the CMIP5 climate models. The color shading indicates the fraction of the models whose value of PCK agrees in sign with the model-mean value (shown in Figure 7). Shown are the seasonally averaged results for: December-February (DJF, left panel) and June-August (JJA, right panel).

Looking at the PCKs across the individual models (Figure 8 provides the results for DJF as an example), there are subsets of models that present qualitatively similar large-scale orientations of relative increases and decreases – but each model PCK carries with it important, unique features that are commensurate in spatial scale to the South Africa sub-regions of interest. From the remaining pool of CMIP5 models, there are PCKs that indicate a very distinct model response. These considerations raise a question as to the overall pattern of model "consensus". To assess a landscape of consensus, we first perform a point-wise calculation of the standard deviation across the CMIP5 models' PCK values we obtained on the 2˚x2.5˚ common grid resolution (Figure 9). For all seasons across the South Africa regions, we find that this metric of consensus follows an east-west gradient with the lowest values of

inter-model standard deviation confined to the WSoAfr region. The ESoAfr region consistently displays the largest degree of model differences, that can be up to an order of magnitude larger than values typically found across the WSoAfr region. The CSoAfr region is typically oriented along a distinct gradient between these contrasting features along its eastern and western flanks. Given this, the consistency in the sign of the PCKs (Figure 10) is also considered. In alignment with the relatively low inter-model standard deviations, the strongest extent of "consensus" in the sign of precipitation change is located over the WSoAfr region (seen in JJA) with over 75% of the models in agreement (to the sign of the model-mean). While all the regions show that at least 50% of the models agree in sign for JJA, in DJF the CSoAfr region as well as the northern portion of ESoAfr show a lack of sign agreement (i.e. less than 50% of the models agree in sign to the model-mean value).

Taken altogether within the construct of the HFD framework (summarized by Eq. 1), the presented regional distinctions in PKCs essentially underscore the inherent risk-based nature of climate change and its effect on regional precipitation change. An additional consideration is the contribution of the MESM's zonal-based projections of change, and in particular, their alignment with the landscapes of the PCKs (Figures 11 and 12 summarize for DJF and JJA, respectively). For the summer season (DJF), the preponderance of MESM's zonal projections (i.e. most if not all the inter-quartile range) produces a decrease in precipitation rates. The only exception is the southern-most latitude of the MESM model that covers South Africa, yet even for this zonal band the interquartile range spans both increased and decreased precipitation – and will play an important factor into the resultant meta-ensemble outcomes. Conversely, for JJA the MESM profiles predominantly project increased precipitation rates, with the exception of the northern-most latitudes that intersect with the ESoAfr region. Here, a complex combination exists of predominantly decreased zonal precipitation rates with a model-mean PCK indicating an enhanced reduction in precipitation rate, but with large inter-model scatter and weak sign agreement of PCKs. Further, the preponderance of the zonal trends to one sign of change is minimized and the central tendency of change is decreased by the scenarios of stronger climate targets (i.e. the 2C and 15C scenarios). This again underscores the risk-based nature of this assessment framework, and the next section presents a more quantitative inspection of how these compounding effects result in a distribution of outcomes across the regions of interest.

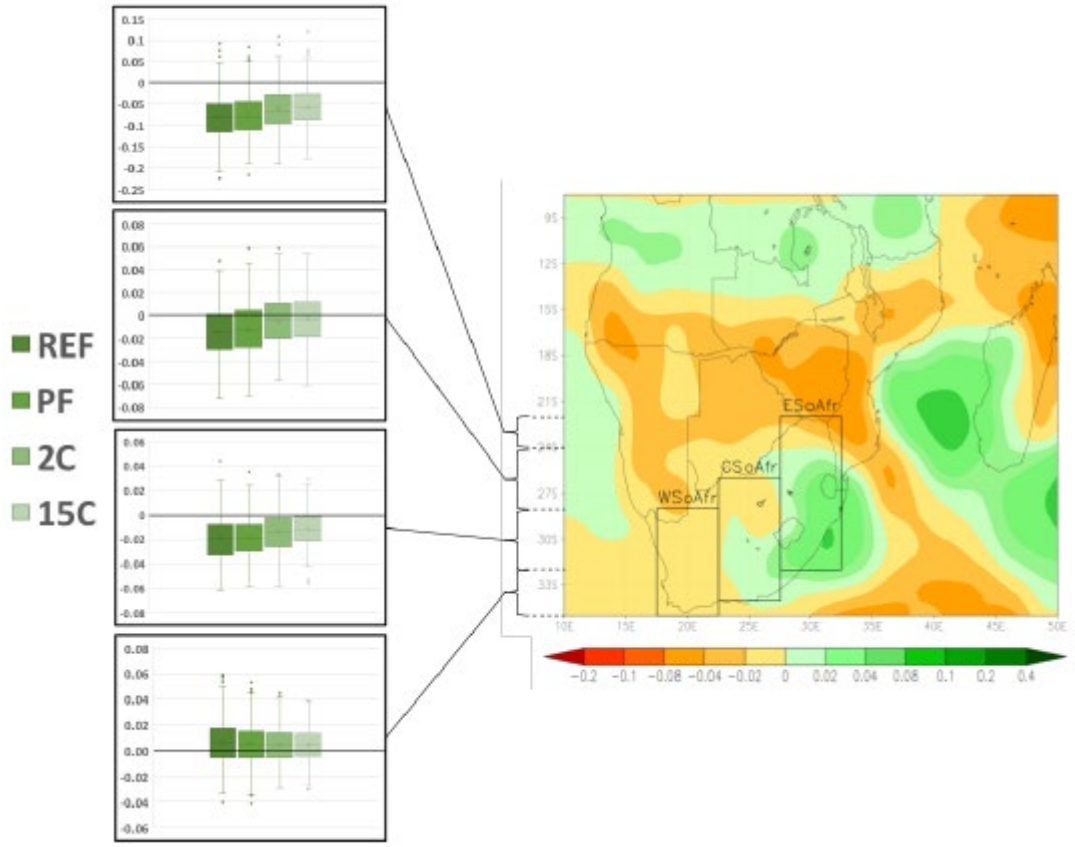

Figure 11: Summary of the contributing model elements of the Hybrid Frequency Distribution (HFD) framework – highlighting the results obtained for the three regions of interest across South Africa (WSoAfr, CSoAfr, and ESoAfr). The right frame shows the model-averaged pattern-change kernel (PCK) for the December-February seasonal mean (also shown in Figure 7). The left frames summarize the distribution of outcomes from the MIT Earth System Model (MESM). Shown are the results from the four scenarios of change performed by the MIT Integrated Global System Model (IGSM) framework: Reference (REF), Paris Forever (PF), and the 2°C and 1.5°C climate targets (2C and 15C, respectively). Each panel on the left corresponds to a latitude band of the MESM outputs and is aligned by the brackets to the left of the PCK map. The ensemble results of each MESM scenario are presented as whisker plots shown the median, interquartile, and min/max – with "outliers" (exceeding 2.5 times the interquartile range from the median) denoted by cross-hairs.

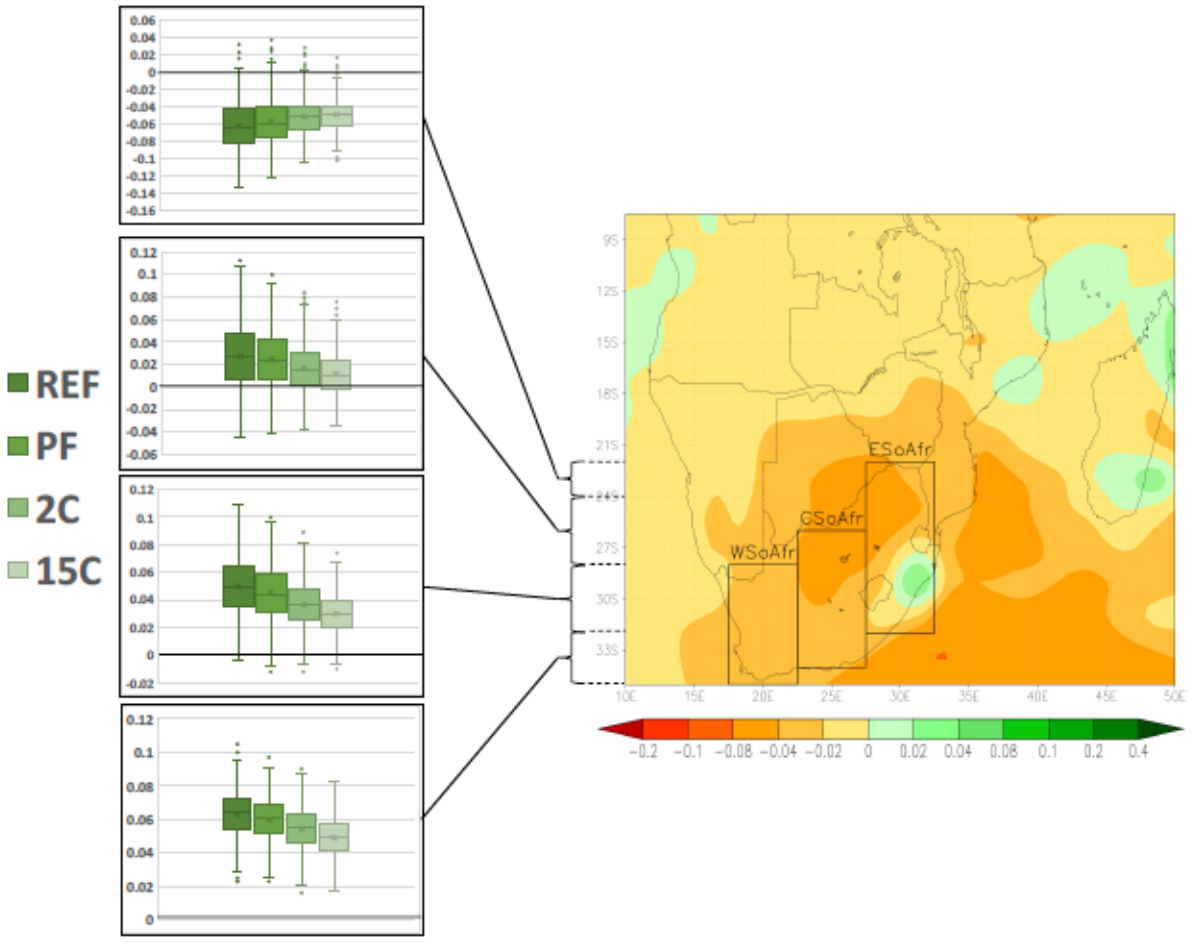

Figure 12: Summary of the contributing model elements of the Hybrid Frequency Distribution (HFD) framework – highlighting the results obtained for the three regions of interest across South Africa (WSoAfr, CSoAfr, and ESoAfr). The right frame shows the model-averaged pattern-change kernel (PCK) for the June-August seasonal mean (also shown in Figure 7). The left frames summarize the distribution of outcomes from the MIT Earth System Model (MESM). Shown are the results from the four scenarios of change performed by the MIT Integrated Global System Model (IGSM) framework: Reference (REF), Paris Forever (PF), and the 2°C and 1.5°C climate targets (2C and 15C, respectively). Each panel on the left corresponds to a latitude band of the MESM outputs and is aligned by the brackets to the left of the PCK map. The ensemble results of each MESM scenario are presented as whisker plots shown the median, interquartile, and min/max – with "outliers" exceeding 2.5 times the interquartile range from the median) denoted by cross-hairs.

2.4 Hybrid frequency distributions

2.4.1 Mid-century changes

For all the regions considered and (averaged) through the mid-century, there is a very high likelihood that seasonally-averaged surface-air temperatures will warm to a level that is salient relative to historical variations (Figure 13). As previously discussed (Section 2.1), the threshold of salience is judged against observed climatological variability (Table 1), and we set a value of 2 standard deviations to the seasonally-averaged decadal-mean quantities (blue shaded regions in Figure 13) – at or beyond which any change is regarded as "salient". In the strict sense, this is not an indication of statistical significance but when considering any variable that is aligned with a Gaussian distribution (such as surface-air temperature) the ±2 standard deviation range would span 95% of the total population of values. Therefore, by this measure, a temperature change of this magnitude (and higher) directly associated with anthropogenic emissions lies among the severe-to-extreme climatological population.

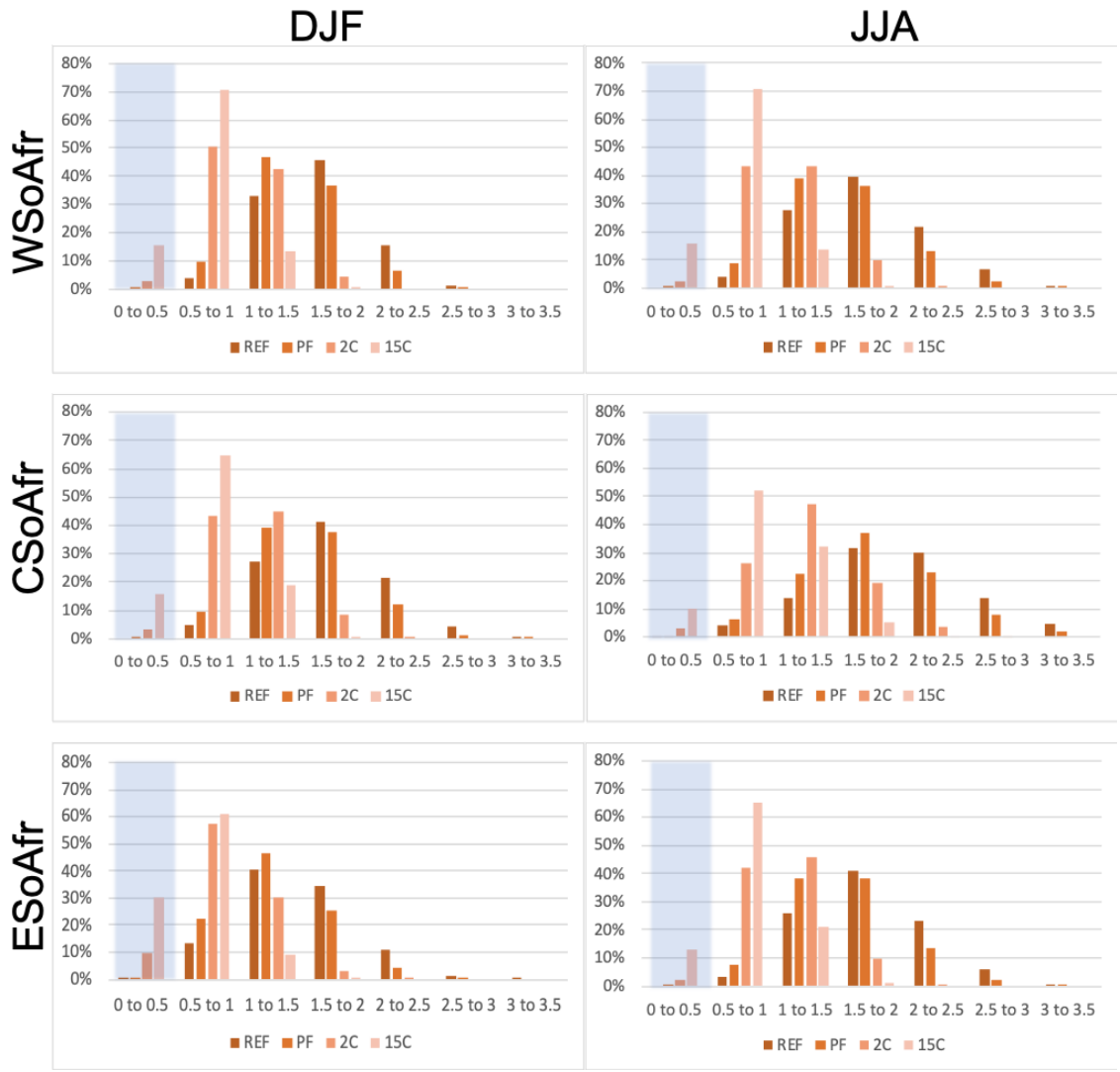

Figure 13. Hybrid frequency distributions (HFDs) of decadal averaged December-February (DJF, left panels) and June-August (JJA, right panels) surface-air temperature change (units in ˚C). The HFDs are constructed for area-averaged quantities of the three sub-regions of South Africa (WSoAfr – top panels, CSoAfr – middle panels, and ESoAfr – bottom panels). Shown are the decadal-averaged changes spanning 2050-2059 relative to the last decade of the 20 century. In each panel, results are provided for the four future scenarios performed by the MIT Integrated Global System Model (IGSM) framework: Reference (REF), Paris Forever (PF), as well as the 2˚C and 1.5˚C climate targets (2C and 15C, respectively). Refer to text for details of the IGSM scenarios performed. In addition, the blue shaded region denotes the bin for which changes in temperature are less than 2 times the standard deviation estimated from observations spanning the 1979-2019 period (presented in Table 1).

In view of this, the results from the HFDs indicate that in all futures considered except the 15C scenario, over 95% of the total population of outcomes result in temperature changes above the level of salience (Figure 13, all panels). Most notably, in all but one of regions and seasons considered (ESoAfr in summer), the REF and PF scenarios show that at least 50% of their distributions result in temperature changes that are at least triple in magnitude to the salience threshold. These likelihoods are substantially reduced in the 2C scenario, with most regions and seasons showing at most 10% of the population remaining (in one case only, CSoAfr in winter, remains at 25%) within the tripled-salience regime. For the 15C scenario, the likelihood of these conditions is nearly eliminated (total portion of distribution at or below 5%). Among the more striking of results is that for the 15C scenario, the most likely temperature change (with greater than 50% of all the outcomes for all regions) is just above the

level of salience and more closely aligned with historical temperature variations. In addition, at least 10% of the population of the regional, seasonal temperature changes from the 15C scenario have values that are commensurate to historical variability (i.e. below salience level).

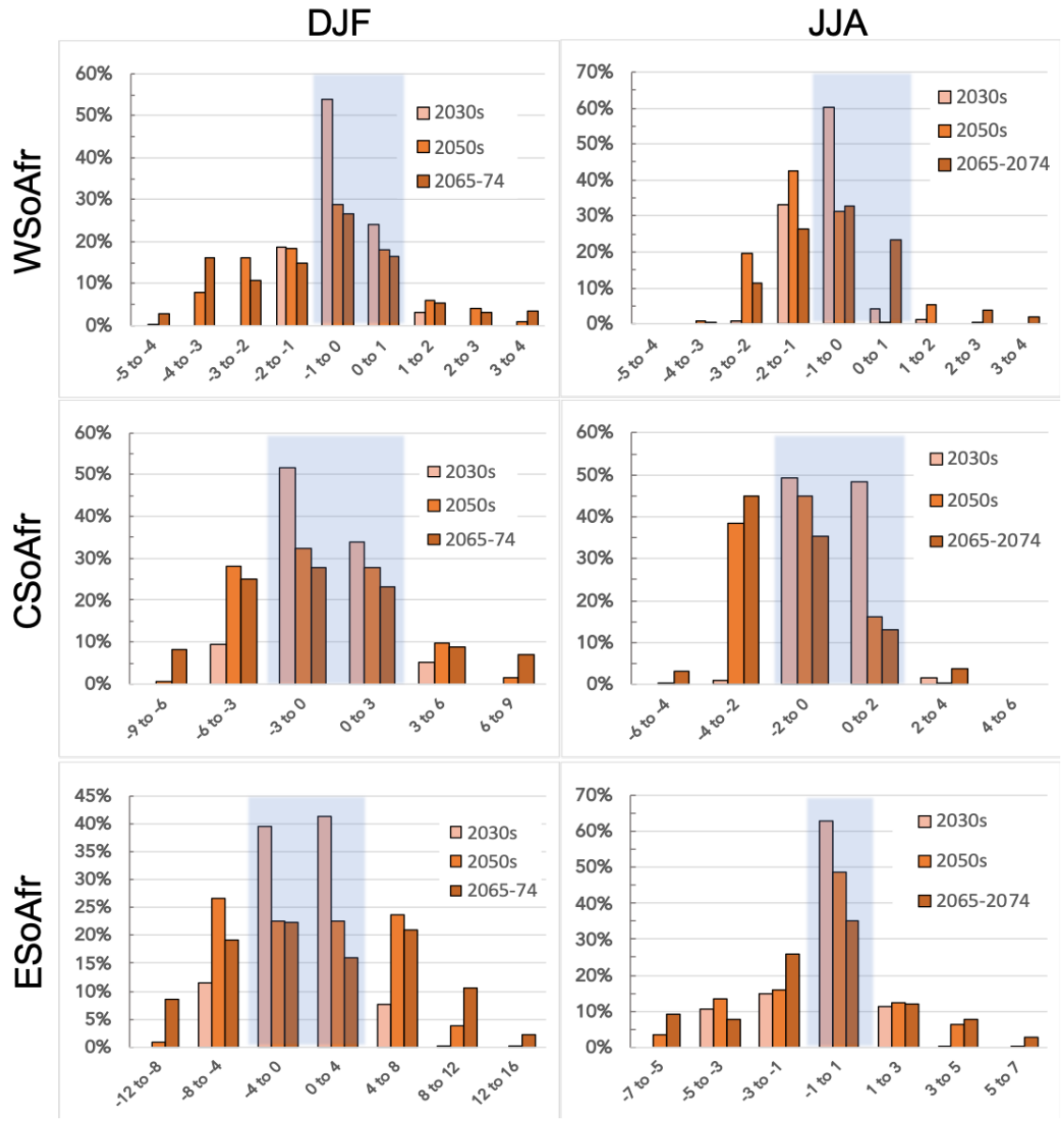

Figure 14. Hybrid frequency distributions (HFDs) of decadal averaged December-February (DJF, left panels) and June-August (JJA, right panels) precipitation change (units in mm/decad, decad=10 days). The HFDs are constructed for area-averaged quantities of the three sub-regions of South Africa (WSoAfr – top panels, CSoAfr – middle panels, and ESoAfr – bottom panels). Shown are the decadal-averaged changes spanning 2030-2039 (2030s), 2050-2059 (2050s), and 2065-74 relative to the last decade of the 20 century. Results are presented for the Reference (REF) scenario performed by the MIT Integrated Global System Model (IGSM) framework. Refer to text for details of the IGSM scenarios performed. In addition, the blue shaded region denotes the bin for which changes in precipitation are less than 2 times the standard deviation estimated from observations spanning the 1979-2019 period (presented in Table 1).

As previously noted in Section 2.3.2, the precipitation pattern-changes across the CMIP5 models differ in sign and structure both across and within the sub-regions of interest. Therefore, the resultant HFDs will (necessarily) reflect likelihoods of both increased and decreased change. Similar to precipitation, we prescribe a degree of salience in order to provide a quantitative judgement on the magnitude of change. Additionally, the relative preponderance of "salient" changes toward drier or wetter

precipitation rates is also gauged under the recognition that equal chances of a dry or wet future would be the equivalent to a proverbial "coin-toss" as to how one should view the risk of change. Under these considerations, the expected changes in precipitation by mid-century (Figure 14, "2050s" results) and into the latter half of the 21st century (Figure 15) indicate that there is a greater risk of a "salient" decrease in precipitation for the WSoAfr and CSoAfr regions for both the summer (DJF) and winter seasons (JJA). In the REF scenario by mid-century, the portion of the distribution with decreased DJF precipitation change is about 3 times that of increased precipitation. For JJA precipitation, this relative preponderance is more pronounced with the distributions' portion of precipitation decreases quadruple to that of decreases. For ESoAfr, these distinctions are largely absent at mid-century (Figure 14, 2050s results) with only a marginally elevated number of outcomes with decreased precipitation (as opposed to increases) during the winter season (JJA), and for the summer the likelihood of decreased or increased precipitation is nearly equal. This feature of the ESoAfr results persists through all of the scenarios considered (not shown). Going into the latter half of the 21st century the likelihood of decreased precipitation change becomes prevalent, yet the largest likelihood of salient decrease has magnitude of change just slightly larger than historical variability.

2.4.2 The evolution of risk and impact of climate targets to abatement

As shown for the temperature change risks at mid-century (Figure 13), there is a very clear impact of the more aggressive climate target scenario at reducing (and nearly eliminating) the risk of the very salient (as given by our metrics) temperature changes. Stemming from the diversity in the modeled precipitation response patterns (Section 2.3), and that precipitation change is not a positive definite change process as the case for temperature, the impacts of climate-target scenarios reducing risks in precipitation change exhibit different characteristics in their behavior. Whether considering the time-dependent (e.g. Figure 14) or scenario-dependent (e.g. Figs. 13 and 15) behavior, the HFDs of precipitation-change primarily respond by broadening and/or tightening of the range of outcomes, and as previously noted, in a number of cases the skewness (or relative preponderance toward positive or negative change) is distinctly altered. Consistent to this behavior is the substantial portion of the distribution still contained within the range of changes that are not regarded as "salient" (within the construct of our analyses). This is quite consistent with the variety and diversity of landscapes in the strength and sign of the precipitation PCKs (Section 2.3) across and within the three regions of focus. Because of this, there will exist a portion of the distribution that will contain weak PCKs, as well as weak sensitivities and trends – all contributing to a fraction of the HFDs with a persistently weaker and more slowly evolving change in the regionally-averaged precipitation. Looking into the latter half of the 21st century (Figure 14 shows results for 2065-2074 seasonal averages), the impact of the more aggressive climate targets to reducing the evolving risks in the REF and PF scenarios is evident. For both the WSoAfr DJF and CSoAfr JJA cases, 45-50% of their REF and PF distributions indicate salient decreases in precipitation. This first underscores that even going into the latter half of the 21st century, current international commitments put forth by the Paris Agreement does not have any impact to reducing this risk. It is with the more aggressive climate target scenarios (2C and 15C) that considerable reductions in risk are seen. Under the 15C scenario, only 5% of CSoAfr JJA precipitation change remains outside the salience regime – a nearly tenfold decrease in the likelihood of change from the REF scenario. The 2C scenario still results in a sizable decrease down to 15% (a threefold decrease). For WSoAfr DJF precipitation, the overall impact of the risk in salient change is not as prominent (likelihood is halved), however both the 2C and 15C scenarios eliminate the occurrence of the largest decreases in precipitation. Overall, the impact of the 15C scenario to reducing risk is most prominently seen when comparing its evolution of risk to that seen in the REF scenario (Figure 16). For all regions and in both summer and winter, the HFDs of precipitation change between the REF scenario in the 2030s compared to the 15C scenario in the 2065-2074 period are nearly identical, and in most cases the likelihood of precipitation changes that aren't considered salient are more likely in the 15C scenario. Thus, this underscores a striking aspect of the 15C scenarios, in that the overall risks to precipitation change, are delayed by about three decades.

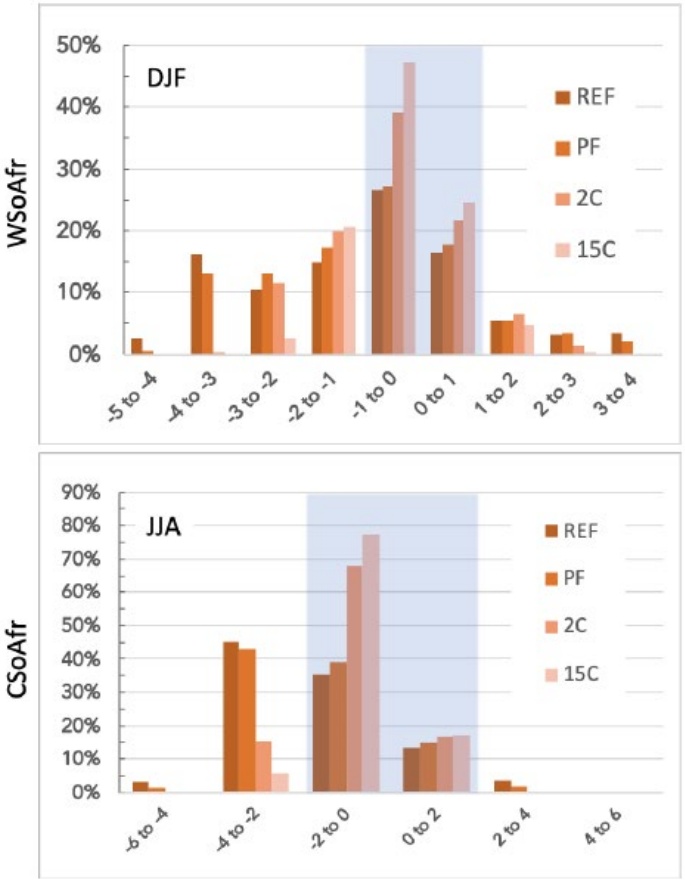

Figure 15. Hybrid frequency distributions (HFDs) of decadal-averaged precipitation change (units in mm/decad, decad=10 days) spanning 2065-2074 relative to the last decade of the 20th century. Top panel presents results for the seasonal averaged December-February (DJF) and areaaveraged WSoAfr region, and the bottom panel presents the seasonal average June-August (JJA), area-averaged CSoAfr region. In each panel, results are provided for the four future scenarios performed by the MIT Integrated Global System Model (IGSM) framework: Reference (REF), Paris Forever (PF), as well as the 2°C and 1.5°C climate targets (2C and 15C, respectively). Refer to text for details of the IGSM scenarios performed. In addition, the blue shaded region denotes the bin for which changes in precipitation are less than 2 times the standard deviation estimated from observations spanning the 1979-2019 period (presented in Table 1).

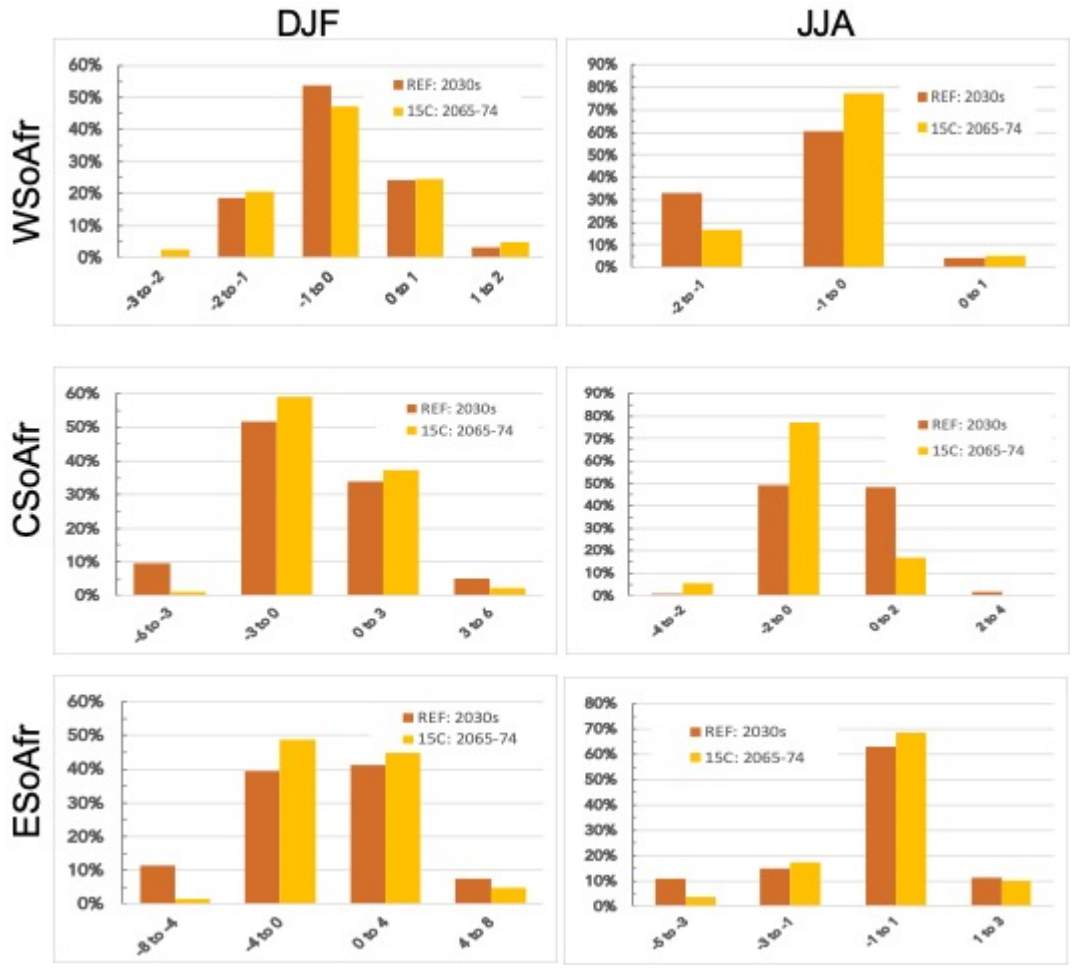

Figure 16. Hybrid frequency distributions (HFDs) of decadal averaged December-February (DJF, left panels) and June-August (JJA, right panels) precipitation change (units in mm/decad, decad=10 days) with respect to the last decade of the 20th century. The HFDs are constructed for area-averaged quantities of the three sub-regions of South Africa (WSoAfr – top panels, CSoAfr – middle panels, and ESoAfr – bottom panels). In each panel, a comparison is presented between the HFDs from two scenarios simulated by the MIT Integrated Global System Model (IGSM) and spanning different decadal periods: the Reference (REF) scenario for the 2030-2039 (2030s) decadal-averaged change versus that from the 1.5˚C (15C) scenario for the 2065-2074 decadal-averaged change. Refer to text for details of the IGSM scenarios performed.

3 SUMMARY REMARKS

In this study, we have presented risk-based results derived from large ensembles of projected changes in seasonal precipitation and near-surface air temperature over South Africa. The ensemble procedure combines, via a Taylor expansion, regional patterns of emerging climate responses from the CMIP5 climate models with the MIT-IGSM, an intermediate complexity earth-system model coupled to a global economic model that evaluates uncertainty in socio-economic growth, anthropogenic emissions, and global environmental response. Given its computational efficiency, the IGSM can be run for large ensembles (e.g. 400 members in this study) to explore the range of possible global climate responses that result from human and natural forcings. In this study, the numerical experimentation with the IGSM included four scenarios of future climate and socio-economic development in order to span a range of possible global actions to abate greenhouse gas emissions over the coming century. When combined with the CMIP5 regional patterns of climate response (i.e. pattern-change kernels), the resultant meta-ensembles (1,000s of members) are used to create "hybrid frequency distributions"

(HFDs) in order to examine the evolution of climate and the extent to which global actions can abate or avoid changes that are regarded as hazardous.

In terms of the regional patterns of climate model responses to anthropogenic drivers (i.e. emissions), the CMIP5 behavior is largely consistent in the land-sea contrast to their surface-air temperature response patterns. The majority of models impose a relatively stronger warming over land. There are, however, isolated exceptions that primarily stem from the influence of maritime climate, which tend to buffer the warming, and these impacts are seen along coastlines. Precipitation exhibits much more diversity in the CMIP5 patterns of response, and this underscores the necessity of taking a risk-based approach in order to identify the preponderant and salient changes.

We evaluated the HFDs of surface-air temperature and precipitation averaged over three regions across South Africa: western (WSoAfr), central (CSoAfr), and eastern (ESoAfr) South Africa. These regions were drawn to align with some of the key features in the observed climate as well as the characteristics and model consensus of the CMIP5 patterns of response. Across all these regions, we find that by mid-century unless stronger measures are put into force that set stricter climate targets, summer and winter averaged temperatures will increase (i.e. over 95% of the REF and PF scenario member simulations) beyond the current climate's variability. In addition, there is a strong likelihood (nearly 50% and higher of the REF and PF scenario member simulations) that temperatures will rise considerably higher than the current climate's range of variability (threefold increase over the current climate's two-standard deviation range of variability). The HFD scenarios that consider more aggressive global climate targets (e.g. 2C and 15C scenarios) all but eliminate the risk of these acutely salient temperature increases. For precipitation, the evolving nature of the regional risks exhibits more distinct features across the regions considered. Most notably, for western South Africa, the preponderance of summer precipitation change across the HFD members indicates that there is a considerably greater likelihood that the region will experience reduced precipitation (as opposed to increased) by mid-century even under current global agreements to reduce emissions. However, without these national commitments (under the Paris Agreement) the likelihood of strong decreases in precipitation (i.e. greater than 3 times the current range of variability) is notable (nearly 20% of the REF ensemble simulations, or a 1-in-5 chance). Given the recent severe drought this region has experienced (e.g. Sousa et al, 2018) and the widespread water-efficiency measures put into action to combat the extreme water shortage, the increasing risk of depleted precipitation that these results imply would indicate that such efficiency measures will become more frequently strained and relied upon. Conversely, across eastern parts of South Africa, the distributions of precipitation change show no clear preponderance toward an increase or decrease through mid-century, and it is only towards the end of the 21st century action under the REF scenario are there indications of a greater risk to decreased precipitation.

There is a clear benefit seen within the evolving hydroclimatic risks as a result of strong climate targets, such as limiting the global climate warming to 1.5˚C by 2100. In all of the regions considered, we find that the risk of precipitation changes in the 15C scenario toward the end of this century (2065-2074) is nearly identical to that seen in the REF scenario during the 2030s. The distributions that result from the 15C scenario toward the end of this century indicate that not all risks of salient changes are removed. Yet, an important aspect of this scenario is that there is a 30-year delay in these risks, relative to the trajectory that is more aligned with the scale of current actions to reduce emissions. This 30-year delay would likely prove to be invaluable toward any national efforts that would be assessed as necessary to prepare and adapt to these heightened risks.

The results of these large ensembles are part of an ongoing analyses to assess the risks of climate change on agriculture yield and production, and the intent is to apply these to other impact sectors of the economic, energy, and infrastructure systems as warranted.

REFERENCES

Adler, R. F., Sapiano, M., Huffman, G. J., Wang, J., Gu, G., Bolvin, D., Chiu, L., Schneider, U., Becker, A., Nelkin, E., Xie, P., Ferraro, R., & Shin, D. B. (2018). The Global Precipitation Climatology Project (GPCP) monthly analysis (New Version 2.3) and a review of 2017 global precipitation. *Atmosphere*, *9*(4), 138. https://doi.org/10.3390/atmos9040138

Arndt, C., Kozlitina, J. and Preckel, P.V. (2006), Efficient survey sampling of households via Gaussian quadrature. *Journal of the Royal Statistical Society*: Series C (Applied Statistics), 55: 355-364. doi:10.1111/j.1467-9876.2006.00537.x.

Arndt, C., Chinowsky, P., Fant, C. *et al.* Climate change and developing country growth: the cases of Malawi, Mozambique, and Zambia. *Climatic Change* **154,** 335–349 (2019). https://doi.org/10.1007/s10584-019-02428-3

Broccoli, A. J., N.-C. Lau, and M. J. Nath, 1998: The cold ocean–warm land pattern: Model simulation and relevance to climate change detection. *Journal of Climate,* **11,** 2743–2763.

Chen, Y.-H.H., S. Paltsev, J.M. Reilly, J.F. Morris and M.H. Babiker (2016): Long-term economic modeling for climate change assessment. *Economic Modelling*, 52(Part B): 867–883. (http://www.sciencedirect.com/science/article/pii/S0264999315003193)

Crétat, J., B. Pohl, Y. Richard, and P. Drobinski, 2012: Uncertainties in simulating regional climate of Southern Africa: sensitivity to physical parameterizations using WRF. *Climate Dynamics*, **38**(3-4), 613-634.

Fant C, Gebretsadik Y, McCluskey A, Strzepek K (2015) An uncertainty approach to assessment of climate change impacts on the Zambezi River Basin. Clim Chang 130:35–48

Huffman, G. J., Adler, R. F., Bolvin, D. T., & Gu, G., 2009: Improving the global precipitation record: GPCP Version 2.1. *Geophysical Research Letters*, **36**, 1-5. Available from http://www.agu.org/pubs/crossref/2009/2009GL040000.shtml

Jones, P.D., New, M., Parker, D.E., Martin, S. and Rigor, I.G., 1999: Surface air temperature and its variations over the last 150 years. *Reviews of Geophysics* **37**, 173-199.

Lennard C, Nikulin G, Dosio A and Moufouma-Okia W (2018) On the need for regional climate information over Africa under varying levels of global warming, Environ. Res. Lett., doi:10.1088/1748-9326/aab37b, http://iopscience.iop.org/article/10.1088/1748-9326/aab2b4

Libardoni, A.G., C.E. Forest, A.P. Sokolov and E. Monier (2018): Estimates of climate system properties incorporating recent climate change. *Advances in Statistical Climatology, Meteorology and Oceanography*, 4(1/2),19-36 (doi:10.5194/ascmo-4-19-2018) (https://www.adv-stat-clim-meteorol-oceanogr.net/4/19/2018/)

Meehl, G. A., C. Covey, T. Delworth, M. Latif, B. McAvaney, J. F. B. Mitchell, R. J. Stouffer, and K. E. Taylor, 2007: The WCRP CMIP3 multi-model dataset: A new era in climate change research, *Bulletin of the American Meteorological Society***, 88**, 1383-1394.

Niang, I., O.C. Ruppel, M.A. Abdrabo, A. Essel, C. Lennard, J. Padgham, and P. Urquhart, 2014: Africa. In: *Climate Change 2014: Impacts, adaptation, and vulnerability. Part B: Regional aspects. Contribution of Working Group II to the Fifth assessment report of the Intergovernmental Panel on Climate Change* [Barros, V.R., C.B. Field, D.J. Dokken, M.D. Mastrandrea, K.J. Mach, T.E. Bilir, M. Chatterjee, K.L. Ebi, Y.O. Estrada, R.C. Genova, B. Girma, E.S. Kissel, A.N. Levy, S. MacCracken, P.R. Mastrandrea, and L.L. White (eds.)]. Cambridge University Press, Cambridge, United Kingdom and New York, NY, USA, pp. 1199-1265.

Osborn, T.J. and Jones, P.D., 2014: The CRUTEM4 land-surface air temperature data set: construction, previous versions and dissemination via Google Earth. *Earth System Science Data* **6**, 61-68, doi:10.5194/essd-6-61-2014

Reilly, J., Y-H Chen, Y-H., A. Sokolov, X. Gao, A. Schlosser, J. Morris, E. Monier, S. Paltsev, 2018. Food, water, energy, climate outlook, 2018, MIT Joint Program on the Science and Policy of Global Change, https://globalchange.mit.edu/outlook2018.

Reifen, C., and R. Toumi, 2009, Climate projections: Past performance no guarantee of future skill? *Geophysical Research Letters*, **36**, doi:10.1029/2009GL038082.

Schlosser, C.A., X. Gao, K. Strzepek, A. Sokolov, C.E. Forest, S. Awadalla, W. Farmer (2012): Quantifying the Likelihood of Regional Climate Change: A Hybridized Approach. *Journal of Climate*, 26(10): 3394-3414 (http://dx.doi.org/10.1175/JCLI-D-11-00730.1)

Schlosser CA, Strzepek K (2015) Regional climate change of the greater Zambezi River basin: a hybrid assessment. *Climatic Change*, 130:9–19.

Sokolov, A., Kicklighter, D., Schlosser, A., Wang, C., Monier, E., Brown-Steiner, B., et al. (2018). Description and evaluation of the MIT Earth System Model (MESM). *Journal of Advances in Modeling Earth Systems*, 10, 1759–1789. https://doi.org/ 10.1002/2018MS001277

Sousa, Pedro M.; Blamey, R.; Reason, C.J.C.; Ramos, A.M.; Trigo, R.M. (2018). "The 'Day Zero' Cape Town drought and the poleward migration of moisture corridors". *Environmental Research Letters*. **13** (12): 124025. doi:10.1088/1748-9326/aaebc7.

Taylor, K.E., R.J. Stouffer, G.A. Meehl, 2012: An overview of CMIP5 and the experiment design. Bull. Amer. Meteor. Soc., **93**, 485-498, doi:10.1175/BAMS-D-11-00094.1.

Thomas, T., et al., 2020: Climate change risks to crop yields over southern Africa (tentative title, and forthcoming paper).

Acknowledgments

This work was funded by the IFPRI SA-TIED project with additional support from the Policies, Institutions, and Markets Research Program of the CGIAR. The authors gratefully acknowledge this as well as additional financial support for this work provided by the MIT Joint Program on the Science and Policy of Global Change through a consortium of industrial sponsors and Federal grants. Development of the IGSM applied in this research was supported by the U.S. Department of Energy, Office of Science (DE-FG02-94ER61937); the U.S. Environmental Protection Agency, EPRI, and other U.S. government agencies and a consortium of 40 industrial and foundation sponsors. For a complete list see https://globalchange.mit.edu/sponsors/current.

About the authors

C. Adam Schlosser, Andrei Sokolov, Ken Strzepek, and Xiang Gao are researchers at the Joint Program on the Science and Policy of Global Change, MIT, Cambridge, MA. Tim Thomas and Channing Arndt are at the International Food Policy Research Institute in Washington D.C., where Channing is the Director of the Environment and Production Technology Division.

INTERNATIONAL FOOD POLICY RESEARCH INSTITUTE
A world free of hunger and malnutrition
1201 Eye Street, NW | Washington, DC 20005-3915 USA
T: +1.202.862.5600 | F: +1.202.862.5606
Email: ifpri@cgiar.org | www.ifpri.org
This paper was prepared as an output for the Towards Inclusive Economic Development in Southern Africa (SA-TIED) project and has not been peer reviewed. Any opinions stated herein are those of the authors and not necessarily representative of or endorsed by IFPRI. The boundaries, names, and designations used in this publication do not imply official endorsement or acceptance by the authors, the International Food Policy Research Institute (IFPRI), or its partners and donors.

Copyright © 2020. Remains with author(s). All rights reserved.